FRONTIERS OF PHYSICS

RESEARCH ARTICLE
Volume 18 / Issue 1 / 13303 / 2023

Electronic properties of monolayer copper selenide with one-dimensional moiré patterns

Gefei Niu[1,*], Jianchen Lu[1,*,†], Jianqun Geng[1,*], Shicheng Li[1], Hui Zhang[1], Wei Xiong[1], Zilin Ruan[1], Yong Zhang[1], Boyu Fu[1], Lei Gao[2,‡], Jinming Cai[1,§]

1 Faculty of Materials Science and Engineering, Kunming University of Science and Technology, Kunming 650093, China
2 Faculty of Science, Kunming University of Science and Technology, Kunming 650500, China
Corresponding authors. E-mail: †jclu@kust.edu.cn, ‡lgao@kust.edu.cn, §j.cai@kust.edu.cn
*These authors contributed equally.

Received June 7, 2022; accepted October 11, 2022

ABSTRACT

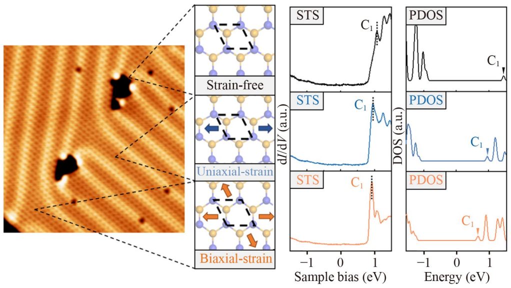

Strain engineering is a vital way to manipulate the electronic properties of two-dimensional (2D) materials. As a typical representative of transition metal mono-chalcogenides (TMMs), a honeycomb CuSe monolayer features with one-dimensional (1D) moiré patterns owing to the uniaxial strain along one of three equivalent orientations of Cu(111) substrates. Here, by combining low-temperature scanning tunneling microscopy/spectroscopy (STM/S) experiments and density functional theory (DFT) calculations, we systematically investigate the electronic properties of the strained CuSe monolayer on the Cu(111) substrate. Our results show the semiconducting feature of CuSe monolayer with a band gap of 1.28 eV and the 1D periodical modulation of electronic properties by the 1D moiré patterns. Except for the uniaxially strained CuSe monolayer, we observed domain boundary and line defects in the CuSe monolayer, where the biaxial-strain and strain-free conditions can be investigated respectively. STS measurements for the three different strain regions show that the first peak in conduction band will move downward with the increasing strain. DFT calculations based on the three CuSe atomic models with different strain inside reproduced the peak movement. The present findings not only enrich the fundamental comprehension toward the influence of strain on electronic properties at 2D limit, but also offer the benchmark for the development of 2D semiconductor materials.

Keywords CuSe monolayer, scanning tunneling microscopy, strain, electronic bandgap, electronic property

1 Introduction

Two-dimensional (2D) materials have drawn much attention in the past few years, owing to their novel physical and chemical properties and potential applications in various fields [1–7]. As a member of the 2D material family, monolayer transition metal mono chalcogenides (TMMs) have sparked tremendous interest in recent years [8–17]. Monolayer CuSe with graphene-like honeycomb lattice, a typical representative of 2D TMMs, had been theoretical predicted to possess 2D Dirac nodal line fermion (DNLF) protected by mirror reflection symmetry, making CuSe monolayer a new platform to study 2D DNLFs and potential applications in the field of high-speed low-dissipation devices [12, 16].

Moiré patterns formed by the lattice mismatch between the attached 2D materials and underlying substrates can introduce additional periodic potential field into 2D materials, which are expected to efficiently modulate the electronic properties of 2D materials [18–21]. Normally, the symmetry of moiré patterns is highly related to the 2D materials and the substrate.

Higher Education Press

https://doi.org/10.1007/s11467-022-1211-0

For instance, the 3-fold symmetry of graphene grown epitaxially on the 6-fold symmetry of Ru(0001) substrate will produce the 6-fold symmetry of moiré patterns [22]. However, CuSe monolayer grown on Cu(111) substrate presents a completely different situation. Due to the strong interaction between CuSe monolayer and Cu(111) substrate, the honeycomb lattice structure of CuSe monolayer tends to be stretched in one direction by a uniaxial strain, resulting in the formation of an unprecedented one-dimensional (1D) moiré patterns [12]. It had been reported that 2D materials with 1D moiré patterns can host 1D topological interface mode arrays at smooth interfaces between local regions of distinct topological properties across the moiré [23–24]. CuSe monolayer with 1D moiré patterns hosts a uniaxial strain. It is natural to ask how strain affects the electronic properties of CuSe monolayer on the Cu(111) substrate.

Here, we thoroughly investigated the effect of strain on the electronic properties of the CuSe monolayer with 1D moiré patterns on the Cu(111) substrate by a combination of scanning tunneling microscopy/spectroscopy (STM/S) and density functional theory (DFT). Our results show that three distinct regions of CuSe monolayer with 1D moiré patterns on the Cu(111) substrate have similar electronic properties, but a slightly different peak intensity at –0.66 eV, presenting a periodically modulated electronic properties of CuSe monolayer. We observe the domain boundary between two different orientations of 1D moiré patterns, and confirm that the boundary region suffers from a biaxial strain. STS measurements for the uniaxial strain, the biaxial strain and the strain-free regions (near the line defect) reveal the first peak in the conduction band will move slightly. The calculated local density of states (LDOS) for three models of CuSe monolayer with different strains reproduced the experimental STS spectra.

2 Methods

2.1 Sample preparation and characterization

Our experiment was performed by a commercial LT-STM/STS system (Scienta Omicron) operating at a base pressure below 1.0×10^{-10} mbar, equipped with a standard molecular beam epitaxy (MBE) system. All STM and STS results were acquired at liquid-helium temperature (4.2K). Cu(111) single crystal substrate was cleaned by cycles of argon-ion sputtering and subsequent annealing to 773 K. The Cu(111) surface quality was clarified through STM imaging. High purity Se powder (99.99%, Sigma-Aldrich) evaporated from a Knudsen cell at ~393 K was deposited onto the room-temperature Cu(111) substrate. Subsequently, the sample was annealed to 473 K for 20 min to grow CuSe monolayer with 1D moiré patterns by a one-step selenization of Cu(111) substrate. All STM images were acquired in a constant-current mode, using an electrochemically etched tungsten tip. All bias voltages were applied to the sample with respect to the tip. The Nanotec Electronica WSxM software was used to process the STM images [25]. $\mathrm{d}I/\mathrm{d}V$ spectra were recorded by a lock-in amplifier with a bias modulation of 10 mV and a frequency of 599 Hz.

2.2 First-principle calculations

First-principles calculations were performed by using the Vienna ab initio simulation package (VASP). The projector augmented wave method was employed to describe the core electrons. The local density approximation (LDA) was used for exchange and correlation. The rotationally invariant LDA+U formalism was used and U_{eff} was chosen as 6.52 eV for Cu. Electronic wavefunctions were expanded in plane waves with a kinetic energy cutoff of 400 eV. The structures were relaxed until the energy and residual force on each atom were smaller than 10^{-4} eV and 0.02 eV·Å^{-1}, respectively. The k-points sampling was $16 \times 16 \times 1$, generated automatically with the origin at the Γ-point. The vacuum layer of the model was larger than 15 Å.

3 Results and discussion

The CuSe monolayer with 1D moiré patterns is grown by a direct one-step selenization of a Cu(111) substrate at low Se coverage as described in our previously published papers [11, 12, 14, 16]. Due to the uniaxially strained honeycomb lattice of CuSe monolayer with respect to the Cu(111) substrate, large-scale and well-defined 1D moiré patterns are formed [12]. Moreover, some mirror twin boundaries locate on the 1D moiré patterns of the CuSe monolayer, which will make the CuSe lattice at both ends of the line defects mirror-symmetrically arranged (Fig. S1). Figure 1(a) shows an atomically resolved STM image of the CuSe monolayer endowed with a well arrangement 1D moiré patterns [12, 16]. Based on the space variation between bright stripes [see a line-profile in Fig. S2(c)], CuSe surface could be divided into three regions: deep valley (DV), shallow valley (SV) and bright ridge (BR) regions, as shown in Fig. 1(a). For clarity, the three regions are marked with three straight colored dashed lines in the lower right corner of Fig. 1(a). To investigate the electronic properties of the CuSe monolayer, we then performed the STS characterization. Figure S2(b) shows three waterfall plots of normalized $\mathrm{d}I/\mathrm{d}V$ curves along the gradient arrows in the three distinct regions in Fig. S2(a), indicating a uniform electronic distribution in each region. Figure 1(b) shows three representative $\mathrm{d}I/\mathrm{d}V$ curves collected at blue, green and red dots in three regions, respectively. All three curves show the same

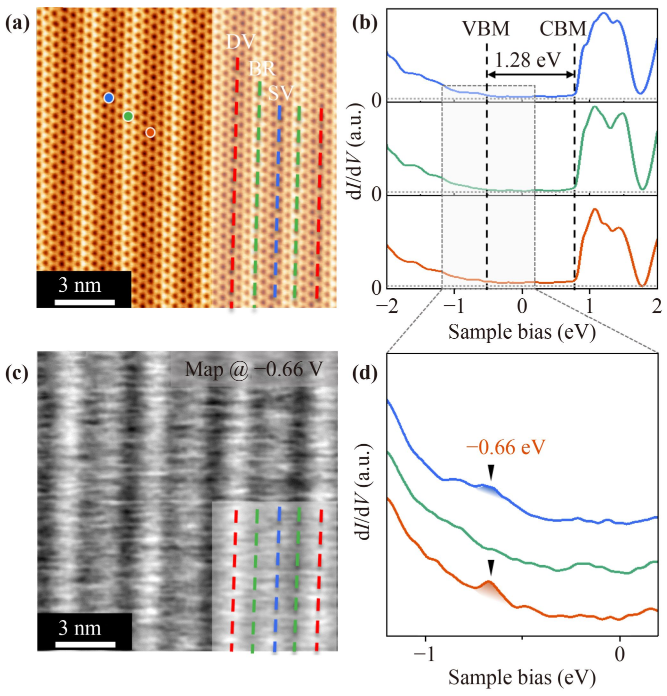

Fig. 1 Electronic properties of CuSe monolayer with 1D moiré patterns. **(a)** An atomically resolved STM image of 1D moiré patterns CuSe monolayer with hexagonal honeycomb lattice. **(b)** Three dI/dV curves collected at different positions which are marked by blue, green and red dots in (a). **(c)** A corresponding dI/dV map obtained at the energy of –0.66 V. Red, blue and green dashed lines in (a) and (c) indicate three different regions in 1D moiré patterns. **(d)** Zoom-in dI/dV curves from a gray square in (b). Two black triangles represent a peak at –0.66 V. Scanning parameters: (a) V_s = –0.42 V, I_t = 300 pA; (b) V_s = 1.5 V, I_t = 400 pA, V_{rms} = 10 mV; (c) V_s = –0.66 V, I_t = 300 pA.

semiconducting behavior with valence band maximum (VBM) located at –0.52 eV and conductance band minimum (CBM) located at 0.76 eV, resulting an electronic bandgap of ~1.28 eV.

Figure 1(d) shows zoom-in dI/dV curves from Fig. 1(b) with the energy range from −1.2 eV to 0.2 eV. Interestingly, the blue and red curves obtained at the SV and DV regions manifest a small peak at –0.66 eV, while the green curve from the BR region has no this feature. Additionally, the peak intensity for the DV region is slightly stronger than that for the SV regions. The peak intensity difference can be clearly identified in a dI/dV map at–0.66 eV [Fig. 1(c)], showing an obvious 1D periodic modulation of the electronic structure for the CuSe monolayer on the Cu(111) substrate. To figure out the physical origin of the –0.66 eV peak, the projected density of states (PDOSs) in different regions are further calculated. As shown in Fig. S3, the –0.5 eV peaks are clearly observed in both blue and red curves in the calculated PDOSs contributed by in-plane orbitals (Se p_x/p_y and Cu $d_{xy}/d_{x^2-y^2}/d_{z^2}$) [Fig. S3(d)], while the green curve had no –0.5 eV peak. The trend of the –0.5 eV peaks in Fig. S3(d) is consistent with that of –0.66 eV peaks in dI/dV curves [Fig. 1(c)], indicating that the –0.66 eV peak in dI/dV curves is mainly contributed by in-plane orbitals of CuSe monolayer at SV and DV regions.

Due to the 6-fold symmetry of Cu(111) substrate, the as-synthesized 1D moiré patterns in the CuSe monolayer manifest three equivalent domains [12]. Figure 2(a) depicts a typical STM image showing a boundary formed by two different orientations of 1D moiré patterns. Interestingly, the partial connection area between two domains shows regularly arranged and continuous six-membered rings (see the high resolution STM image for the domain boundary in Fig. S4b). Figure 2(d) shows three line-profiles along three directions of CuSe monolayer at the domain boundary as indicated by red, green and yellow dashed lines in Fig. 2(a), where the directions of the red and yellow dashed lines are parallel to the orientation of 1D moiré pattern of two domains on both sides of the boundary, respectively. The measured periodicity of CuSe honeycomb lattice in three directions is 0.439 nm (red curve), 0.417 nm (green curve), and 0.435 nm (yellow curve). Obviously, the periodicity in the red and yellow directions is very similar and significantly larger than that in the green direction.

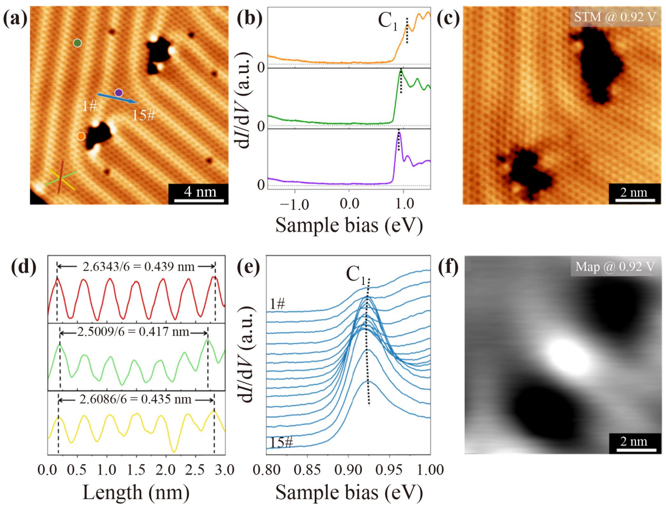

Fig. 2 Atomic structures and electronic properties of domain boundary of CuSe monolayer on Cu(111) substrate. **(a)** A high resolution STM image of the domain boundary. **(b)** dI/dV curves collected at three positions, as indicated by colored dots in (a). Black dashed lines indicate the positions of C_1 peak in the conduction band. **(c, f)** STM image and corresponding dI/dV map at the energy of 0.92 V. **(d)** Three line-profiles at the domain boundary across the red, green, and yellow lines in (a). **(e)** Waterfall plots of dI/dV curves along a blue arrow in (a). A black curved dashed line indicates the C_1 peak movement. Scanning parameters: (a) V_s = 50 mV, I_t = 1.3 nA; (b) V_s = 2 V, I_t = 300 pA, V_{rms} = 10 mV; (c) V_s = 0.92 V, I_t = 300 pA; (e) V_s = 2 V, I_t = 300 pA, V_{rms} = 10 mV; (f) V_s = 0.92 mV, I_t = 300 pA, V_{rms} = 10 mV.

We then confirm that the lattice structure of CuSe monolayer in this area of the domain boundary is stretched by a biaxial strain. However, the domain boundary also exists few large irregularly shaped defects shown in Fig. 2(a). This confirms that the perfect connection between two domains of CuSe monolayer will produce great strain accumulation at the boundary, thus resulting in the formation of large defects. A convincing evidence is that the lattice constant around the irregularly shaped defect in Fig. S4(c) (0.406 nm) is slightly smaller than that in the internal biaxial strain (BS) [0.435 nm in Fig. 2(d)]. It should be noted that thanks to the formed large defects in the domain boundary, the CuSe honeycomb lattice near the large defect will be not affected by strain.

To investigate the effect of strain on the electronic structures of CuSe monolayer, we carried out the differential conductance spectroscopy ($\mathrm{d}I/\mathrm{d}V$) measurements. Figure 2(b) shows three $\mathrm{d}I/\mathrm{d}V$ curves collected from three distinct regions in the Fig. 2(a). The orange curve taken near the edge of a large irregularly shaped defect represents the electronic properties of CuSe monolayer without strain, while the green curve collected from the DV region reflects the electronic properties of CuSe monolayer distorted by uniaxial strain (US), and the purple curve obtained from the domain boundary gives access to the electronic properties of CuSe monolayer distorted by biaxial strain (BS). Although the three curves show similar semiconducting behavior, the first peak labelled by C_1 in conduction band has an obvious movement, as marked by a series of black dashed lines. The C_1 peak locates at 1.06 eV for the strain-free region, while for the US region and BS region, this peak shifts down to 0.95 eV and 0.92 eV, respectively (see Fig. S5 for more $\mathrm{d}I/\mathrm{d}V$ curves near the strain-free region). Additionally, in order to further investigate the movement of C_1 peak, we took a series of $\mathrm{d}I/\mathrm{d}V$ spectra along a blue arrow from one 1D moiré pattern domain to another domain via domain boundary in Fig. 2(a), where the stain in the CuSe monolayer changes from US vis BS to US. Figure 2(e) shows waterfall plots of normalized $\mathrm{d}I/\mathrm{d}V$ curves, and a black curved dashed line describes the changing trend of C_1 peak in conduction band. Evidently, the C_1 peak slightly moves down from 0.93 eV to 0.92 eV and then gradually increases to 0.93 eV, which further confirms the strain can modulate the electronic structures of CuSe monolayer on the Cu(111) substrate. Figures 2(c) and (f) are STM image around the domain boundary and its corresponding $\mathrm{d}I/\mathrm{d}V$ map at 0.92 eV, respectively. It can be clearly found that the electronic states are strongly concentrated in the BS area (domain boundary) at 0.92 eV, in good agreement with STS results in Figs. 2(b) and (e).

In addition to the domain boundaries consisted of two different orientations of 1D moiré patterns of CuSe monolayer on the Cu(111) substrate, we also observed two kinds of line defects formed by mirror-symmetric domains on both sides [Figs. 3(a) and (c)]. Figures 3(b) and (d) are zoom-in STM images of Figs. 3(a) and (c), showing atomically resolved structures of the line defects, respectively. A schematic description of edge terminations of a CuSe hexagonal island is illustrated in Fig. S6, where the Cu-edge and Se-edge are represented by blue and yellow dashed lines, respectively. Figure 3(e) presents a schematic diagram of the line defect formed by two mirror-symmetric CuSe monolayer domains, where the mirror domains can be clearly identified by

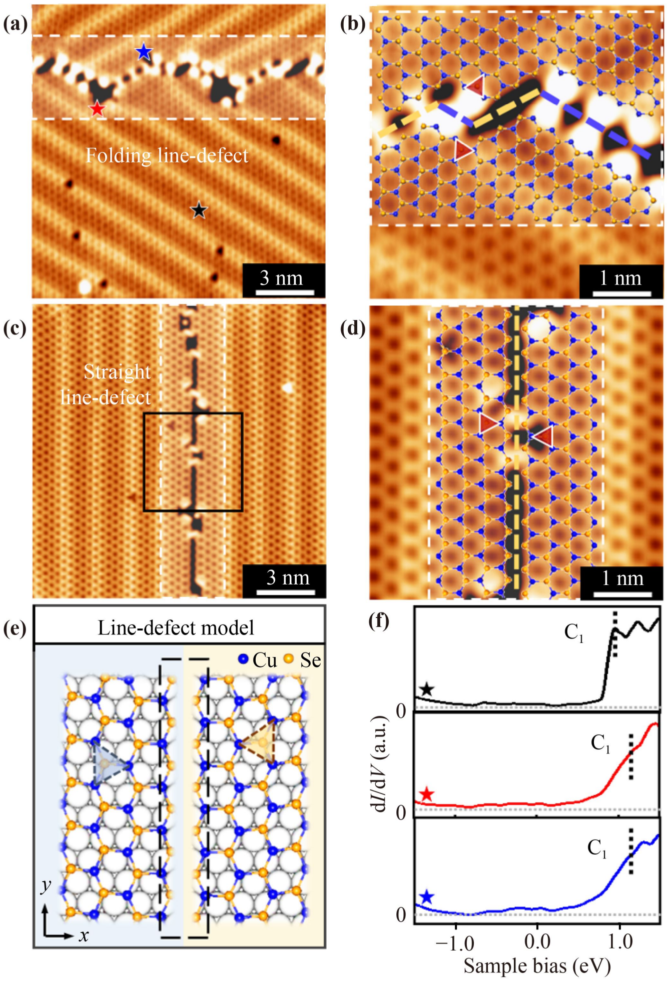

Fig. 3 Line defects in the CuSe monolayer on the Cu(111) substrate. **(a, b)** A large-scale STM image and corresponding high-resolution STM image of the folding line-defect. **(c, d)** A large-scale STM image and corresponding high-resolution STM image of the straight line-defect. Atomic models are covered into (b) and (d) to shed light on the edge termations. **(e)** Schematic description of straight line-defect in CuSe atomic model, where blue and yellwo triangles indicate that the left and right modles are two mirror-symmetric domains. **(f)** $\mathrm{d}I/\mathrm{d}V$ curves taken at three positions, as marked by black, red and blue stars in (a). Scanning parameters: (a) $V_\mathrm{s} = 0.4$ V, $I_\mathrm{t} = 200$ pA; (b) $V_\mathrm{s} = 2$ V, $I_\mathrm{t} = 300$ pA; (c) $V_\mathrm{s} = 0.2$ V, $I_\mathrm{t} = 100$ pA; (d) $V_\mathrm{s} = 0.2$ V, $I_\mathrm{t} = 100$ pA; (f) $V_\mathrm{s} = 2$ V, $I_\mathrm{t} = 400$ pA, $V_\mathrm{rms} = 10$ mV.

blue and yellow triangles. To identify the edge terminations of the observed line defects, we superimpose the atomic models of two mirror domains of CuSe monolayer into Figs. 3(b) and (d). The results show that the edge terminations are an alternate Cu-edge and Se edge in Fig. 3(b), forming a folding line defect, while Fig. 3(d) presents a straight Se edge, forming a straight line defect. In order to study the electronic properties of CuSe monolayer near the line defect, where the lattice structure should be free of strain, we carried out $\mathrm{d}I/\mathrm{d}V$ measurements. Figure 3f shows STS curves taken near the line defect and terrace of CuSe monolayer, as marked by black, red and blue stars in Fig. 3(a). The STS results clearly show the movement of the C_1 peak positions, as indicated by black dashed lines in Fig. 3(g), further confirming that the strain will induce the peak position to move towards downward. In addition, due to the existence of edge dangling bonds outside the defect, the freestanding CuSe has trivial and non-trivial boundary states [12]. However, on the Cu(111) substrate, the edge dangling bond of CuSe is saturated by the Cu(111) substrate, so there is no doubt that it doesn't show the boundary state externally (Fig. S7).

In order to further investigate the electronic properties of monolayer CuSe, we performed first-principles calculations on (1 × 1) CuSe monolayer under strain-free, uniaxial strain (US) and biaxial strain (BS) respectively, as shown in Figs. 4(a)–(c). The magnitude of strain is defined as $\varepsilon = (a\text{–}a_0)/a_0$, where a and a_0 are the lattice constants of the strained and unstrained structures, respectively. According to the published paper, the lattice constants of CuSe monolayer along the orientation of 1D moiré pattern is 7.3% larger than those along other directions [12]. The density of states (DOSs) of CuSe monolayer under strain-free condition is shown in Fig. 4(d). The first peak (C_1) above the Fermi level is about 1.44 eV. Under 7.3% US and 7.3% BS, the C_1 peak shifts left to 0.95 eV [Fig. 4(e)] and 0.66 eV [Fig. 4(f)] respectively, which is in good agreement with the experimental $\mathrm{d}I/\mathrm{d}V$ curves in Fig. 2(b).

To better understand how strain affects the electronic structures of CuSe monolayer, first-principles calculations of CuSe monolayer with US and BS ranging from −5% to 5% were further performed. As shown in Fig. 4(g), the CBM, VBM and Fermi level variations with BS of CuSe monolayer are larger than those with US. Under both US and BS, the CBM and VBM of CuSe monolayer move more with the increasing strain. Furthermore, the differential charge densities of CuSe monolayer under strain-free, 7.3% US and 7.3% BS were also investigated. The differential charge densities of CuSe monolayer under strain-free [Fig. 4(h)] shows charge accumulations between Cu and Se atoms, while charge depletion on Cu and Se atoms, hence demonstrating a covalent bonding character. Under 7.3% US [Fig. 4(i)] and 7.3% BS [Fig. 4(j)], the charge accumulations between Cu and Se atoms and the charge depletions on Cu and Se atoms become less, demonstrating weaker covalent bonding characters which is the main cause of the C1 peak shift to the left. To figure out the physical origin of the C1 peak, the PDOSs of monolayer CuSe under strain-free, 7.3% uniaxial-strain and 7.3% biaxial-strain on Cu(111) are further calculated. As shown in Fig. S8, the C1 peak is mainly dominated by s orbitals of CuSe monolayer.

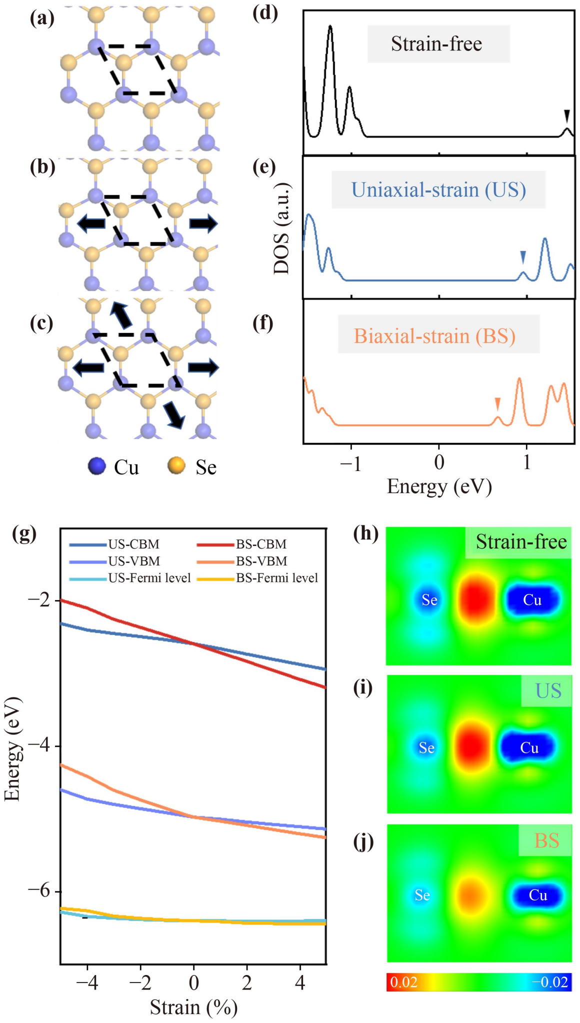

Fig. 4 Atomic configurations and calculated electronic structures of CuSe monolayer. **(a–c)** Atomic configurations of CuSe monolayer under strain-free, 7.3% uniaxial-strain and 7.3% biaxial-strain, respectively. The primitive cell of CuSe monolayer is denoted by the black dotted line. **(d–f)** DOSs of CuSe monolayer under strain-free, 7.3% uniaxial-strain and 7.3% biaxial-strain, respectively. **(g)** CBM, VBM and Fermi level variations under uniaxial-strain and biaxial-strain of CuSe monolayer. **(h–j)** Cross sections of differential charge density (e/Bohr^3) of CuSe monolayer under strain-free, 7.3% uniaxial-strain and 7.3% biaxial-strain, respectively.

4 Conclusion

In summary, we demonstrate the direct investigation of electronic properties of CuSe monolayer on the Cu(111) substrate under different strain conditions, fully characterized by combined STM/STS measurements, and supported by DFT calculations. The uniaxial strain induced 1D moiré patterns produces 1D periodic modulation of electronic structures of CuSe monolayer. Additionally, compared to the uniaxial strain region at the terrace, electronic properties of CuSe monolayer at biaxial strain region existed in the domain boundary and strain-free region found near the line defects show that the first peak in conduction band has a tendency to move in the opposite direction, which has been successfully confirmed by DFT calculations. The results not only enrich the fundamental understanding toward the role of strain in modulating electronic properties of CuSe monolayer, but also lay the foundation for the development of 2D semiconductor materials.

Electronic supplementary material Supplementary materials are available in the online version of this article at https://doi.org/10.1007/s11467-022-1211-0 and https://journal.hep.com.cn/fop/EN/10.1007/s11467-022-1211-0 and are accessible for authorized users.

Acknowledgements This work was supported by the National Natural Science Foundation of China (Nos. 62271238 and 61901200), the Yunnan Fundamental Research Projects (Nos. 202201AT070078, 202101AV070008, 202101AW070010, and 202101AU070043), the Strategic Priority Research Program of Chinese Academy of Sciences (XDB30000000), the Analysis and Testing Foundation of KUST (2021T20170056), and the Dongguan Innovation Research Team Program. Numerical computations were performed on Hefei advanced computing center.

References

1. K. F. Mak, K. L. McGill, J. Park, and P. L. McEuen, The valley Hall effect in MoS_2 transistors, *Science* 344(6191), 1489 (2014)
2. N. Mounet, M. Gibertini, P. Schwaller, D. Campi, A. Merkys, A. Marrazzo, T. Sohier, I. E. Castelli, A. Cepellotti, G. Pizzi, and N. Marzari, Two-dimensional materials from high-throughput computational exfoliation of experimentally known compounds, *Nat. Nanotechnol.* 13(3), 246 (2018)
3. S. Y. Zhu, Y. Shao, E. Wang, L. Cao, X. Y. Li, Z. L. Liu, C. Liu, L. W. Liu, J. O. Wang, K. Ibrahim, J. T. Sun, Y. L. Wang, S. Du, and H. J. Gao, Evidence of topological edge states in buckled antimonene monolayers, *Nano Lett.* 19(9), 6323 (2019)
4. Z. Zhou, F. Yang, S. Wang, L. Wang, X. Wang, C. Wang, Y. Xie, and Q. Liu, Emerging of two-dimensional materials in novel memristor, *Front. Phys.* 17(2), 23204 (2022)
5. Y. H. Mao, H. Shan, J. R. Wu, Z. J. Li, C. Z. Wu, X. F. Zhai, A. D. Zhao, and B. Wang, Observation of pseudogap in $SnSe_2$ atomic layers grown on graphite, *Front. Phys.* 15(4), 43501 (2020)
6. J. X. Lin, Y. H. Zhang, E. Morissette, Z. Wang, S. Liu, D. Rhodes, K. Watanabe, T. Taniguchi, J. Hone, and J. Li, Spin–orbit-driven ferromagnetism at half moiré filling in magic-angle twisted bilayer graphene, *Science* 375(6579), 437 (2022)
7. X. Y. Wang, H. Zhang, Z. L. Ruan, Z. L. Hao, X. T. Yang, J. M. Cai, and J. C. Lu, Research progress of monolayer two-dimensional atomic crystal materials grown by molecular beam epitaxy in ultra-high vacuum conditions, *Acta. Phys. Sin.* 69(11), 118101 (2020)
8. B. Liu, J. Liu, G. Miao, S. Xue, S. Zhang, L. Liu, X. Huang, X. Zhu, S. Meng, J. Guo, M. Liu, and W. Wang, Flat AgTe honeycomb monolayer on Ag(111), *J. Phys. Chem. Lett.* 10(8), 1866 (2019)
9. J. Shah, H. M. Sohail, R. I. G. Uhrberg, and W. Wang, Two-dimensional binary honeycomb layer formed by Ag and Te on Ag(111), *J. Phys. Chem. Lett.* 11(5), 1609 (2020)
10. M. Ünzelmann, H. Bentmann, P. Eck, T. Kißlinger, B. Geldiyev, J. Rieger, S. Moser, R. C. Vidal, K. Kißner, L. Hammer, M. A. Schneider, T. Fauster, G. Sangiovanni, D. Di Sante, and F. Reinert, Orbital-driven Rashba effect in a binary honeycomb monolayer AgTe, *Phys. Rev. Lett.* 124(17), 176401 (2020)
11. X. Lin, J. C. Lu, Y. Shao, Y. Y. Zhang, X. Wu, J. B. Pan, L. Gao, S. Y. Zhu, K. Qian, Y. F. Zhang, D. L. Bao, L. F. Li, Y. Q. Wang, Z. L. Liu, J. T. Sun, T. Lei, C. Liu, J. O. Wang, K. Ibrahim, D. N. Leonard, W. Zhou, H. M. Guo, Y. L. Wang, S. X. Du, S. T. Pantelides, and H. J. Gao, Intrinsically patterned two-dimensional materials for selective adsorption of molecules and nanoclusters, *Nat. Mater.* 16(7), 717 (2017)
12. L. Gao, J. T. Sun, J. C. Lu, H. Li, K. Qian, S. Zhang, Y. Y. Zhang, T. Qian, H. Ding, X. Lin, S. Du, and H. J. Gao, Epitaxial growth of honeycomb monolayer CuSe with Dirac nodal line fermions, *Adv. Mater.* 30(16), 1707055 (2018)
13. J. Lu, L. Gao, S. Song, H. Li, G. Niu, H. Chen, T. Qian, H. Ding, X. Lin, S. Du, and H. J. Gao, Honeycomb AgSe monolayer nanosheets for studying two-dimensional Dirac nodal line fermions, *ACS Appl. Nano Mater.* 4(9), 8845 (2021)
14. X. Wang, Z. Ruan, R. Du, H. Zhang, X. Yang, G. Niu, J. Cai, and J. Lu, Structural characterizations and electronic properties of CuSe monolayer endowed with triangular nanopores, *J. Mater. Sci.* 56(17), 10406 (2021)
15. L. Gao, Y. F. Zhang, J. T. Sun, and S. Du, Band engineering of honeycomb monolayer CuSe via atomic modification, *Chin. Phys. B* 30(10), 106807 (2021)
16. G. Niu, J. Lu, X. Wang, Z Ruan, H. Zhang, L. Gao, J. Cai, and X. Lin, Se-concentration dependent superstructure transformations of CuSe monolayer on Cu(111) substrate, *2D Mater.* 9(1), 015017 (2022)
17. Z. Song, J. Huang, S. Zhang, Y. Cao, C. Liu, R. Zhang, Q. Zheng, L. Cao, L. Huang, J. Wang, T. Qian, H. Ding, W. Zhou, Y. Y. Zhang, H. Lu, C. Shen, X. Lin, S. Du, and H. J. Gao, Observation of an incommensurate charge density wave in monolayer $TiSe_2$/CuSe/Cu(111) heterostructure, *Phys. Rev. Lett.* 128(2), 026401 (2022)

18. K. Tang and W. Qi, Moiré-pattern-tuned electronic structures of van Der Waals heterostructures, *Adv. Funct. Mater.* 30(32), 2002672 (2020)
19. J. Kang, J. Li, S. S. Li, J. B. Xia, and L. W. Wang, Electronic structural moire pattern effects on MoS_2/$MoSe_2$ 2d heterostructures, *Nano Lett.* 13(11), 5485 (2013)
20. K. L. Seyler, P. Rivera, H. Yu, N. P. Wilson, E. L. Ray, D. G. Mandrus, J. Yan, W. Yao, and X. Xu, Signatures of moire-trapped valley excitons in $MoSe_2$/WSe_2 heterobilayers, *Nature* 567(7746), 66 (2019)
21. C. Zhang, M. Y. Li, J. Tersoff, Y. Han, Y. Su, L. J. Li, D. A. Muller, and C. K. Shih, Strain distributions and their influence on electronic structures of WSe_2-MoS_2 laterally strained heterojunctions, *Nat. Nanotechnol.* 13(2), 152 (2018)
22. Y. Pan, H. Zhang, D. Shi, J. Sun, S. Du, F. Liu, and H. Gao, Highly ordered, millimeter-scale, continuous, single-crystalline graphene monolayer formed on Ru (0001), *Adv. Mater.* 21(27), 2777 (2009)
23. Y. S. Bai, L. Zhou, J. Wang, W. J. Wu, L. J. McGilly, D. Halbertal, C. F. B. Lo, F. Liu, J. Ardelean, P. Rivera, N. R. Finney, X. C. Yang, D. N. Basov, W. Yao, X. Xu, J. Hone, A. N. Pasupathy, and X. Y. Zhu, Excitons in strain-induced one-dimensional moiré potentials at transition metal dichalcogenide heterojunctions, *Nat. Mater.* 19(10), 1068 (2020)
24. Q. J. Tong, H. Y. Yu, Q. Z. Zhu, Y. Wang, X. D. Xu, and A. Yao, Topological mosaics in moire superlattices of van Der Waals heterobilayers, *Nat. Phys.* 13(4), 356 (2017)
25. I. Horcas, R. Fernandez, J. M. Gomez-Rodriguez, J. Colchero, J. Gomez-Herrero, and A. M. Baro, WSxM: A software for scanning probe microscopy and a tool for nanotechnology, *Rev. Sci. Instrum.* 78(1), 013705 (2007)